*Nanotechnology Perceptions*
*ISSN 1660-6795*
www.nano-*ntp.com*

# Hot Deformation Behaviour Of AISI 4340 And Constitutive Modelling Of The Flow Behaviour

**M S Mohan[1,a*], Mithun R[1,b], Praveen K[1,c], Linoragul R[1,d], Shynu K[1,e], J Krishnamoorthi[1,f]**

[1]*Department of Metallurgical Engineering, PSG College of Technology, Coimbatore, Tamil Nadu, 641004, India*
[a]*manu.metal@psgtech.ac.in,* [b]*mithunravikms@gmail.com,* [c]*kpraveen735898@gmail.com,* [d]*linoragul04@gmail.com,* [e]*shynu1718@gmail.com,* [f]*jkm.metal@psgtech.ac.in*

AISI 4340 steel, owing to sufficient balance between toughness and strength finds use in bearings, shafts, crankshafts, and landing gears applications. Since the steel under study is subjected to metal forming processes, it necessitates determining the combined effects of various hot working parameters on microstructural evolution. In the current work, the stress strain response of AISI 4340 steel deformed between 900 °C - 1000 °C at various deformation velocities (strain rates) to a maximum true strain of 0.7 was recorded. The peak strength of the steel increased from 217 MPa to 273 MPa, when the processing parameters were varied from 1000 °C, 1 $s^{-1}$ to 900 °C, 1 $s^{-1}$ . The peak stress increased from 118 MPa to 273 MPa when the processing parameters were varied from 900 °C, 0.01 $s^{-1}$ to 900 °C, 1 $s^{-1}$. The constitutive equation for the steel relating stress with process parameters, being the rate of deformation and temperature was determined. The flow curves recorded were fitted to Ludwigson model to determine strength coefficients and strain hardening exponents.

Keywords: 4340; Hot Deformation; Gleeble; Vickers Hardness

## Introduction

AISI 4340 steel finds applications in bearings, gears, shafts, crankshafts, landing gears [1,2] because of good balance between strength and toughness. 4340 has been subjected to hot deformation for producing forged parts and hot rolled products. It is therefore important to understand the optimum processing parameters required for carrying out hot deformation for producing alloy parts without having various instabilities. Hot deformation studies have been performed to improve the workability of many alloys and control the microstructure [3–6]. Shear bands, kink bands, flow localisations [7], grain boundary sliding [8], wedge cracking [8] and deformation bands [9] were the few of the instabilities observed in the microstructures of hot deformed 4340 alloy. Work hardening, and dynamic recrystallization (DRX), depending upon the deformation conditions, occur during hot deformation of 4340 alloy. Since the

austenite phase, the major phase being deformed at elevated temperature, has low stacking fault energy (SFE), the kinetics of dynamic recovery has been found to be sluggish, and therefore dynamic recrystallization occurs during elevated temperature working conditions [10,11]. Needle like ferrite structure formed in the deformed structure resulted in improvement in toughness of the structure [7]. Lukaszek-Solek et al. [9] reported that dynamic recrystallization failed to occur when 4340 was deformed at 900 °C, the rate of deformation being 10 $s^{-1}$. The author [9] reported that recrystallization happened at lower strain rates (< 10 $s^{-1}$). Therefore, the degree of formation of recrystallized grains is influenced by the process parameters. In the hot deformation studies on 4340 steel carried out earlier, the steel was strained to a compressive true strain of 1 [7–9], and the effect of deformation parameters on hardness has not been reported. In the current study, the constitutive equation for AISI 4340 steel relating the peak stress associated with the deformation to the processing parameters (strain rate and temperature) is determined for the alloy deformed to a compressive true strain of 0.7, and the experimentally determined stress-strain curves were fitted with empirical relations[12]. In addition, the Vickers microhardness of the steel was determined to elucidate the effects of hot processing on the deformation response of the processed steel.

## Material and Methods

AISI 4340 steel of dimensions of 10 mm diameter and 91 mm height, was subjected to compressive deformation at hot working temperatures, ranging from 900 °C to 1000 °C with the deformation rates lying in the range from $10^{-2}$ $s^{-1}$ to 1 $s^{-1}$ in the Gleeble® 3500 simulator (Fig.1). The steel specimen (Fig. 1) was heated at a rate of 5 °C/s to the deformation temperature in an argon atmosphere and isothermally held for a duration of seven minutes. Thereafter, the alloy was strained upto a maximum compressive true strain of 0.7 and it was immediately air-cooled. The temperature during the test was recorded using a thermocouple wire (K-Type) spot-welded at the middle section of the 91 mm long specimen, on its surface. Specimens for the scanning electron microscopy (SEM) analysis were machined from the middle section perpendicular to the axis of the deformed specimen and the specimen surface was etched using picric acid. SEM studies were carried out using ZEISS SIGMA Field Emission SEM, in which the secondary electrons were used for imaging. The microhardness testing on deformed specimens was carried out at a load of 10 kg using a Vickers Microhardness Tester.

## Results and Discussion

The elevated temperature stress-strain behaviour of the steel initially demonstrates an increase in stress with the strain which signifies work hardening (Fig. 2). The processes like work hardening and dynamicrecrystallization occur after which a steady state is achieved [9,13,14]. DRX begins to occur when critical value of dislocation density is reached. It is found that, at each of the temperatures of deformation the peak stress increased while the strain rate imposed was raised from the lowest ($10^{-2}$ $s^{-1}$) to the highest values (1 $s^{-1}$). In addition, the magnitude of true strain at

which the peak stress reaches its maximum shifted towards higher strain with increase in strain rate. At each of the strain rates, lowering of peak stress resulted when there was an increase in deformation temperature. The effects of variation in the processing parameters (temperature,

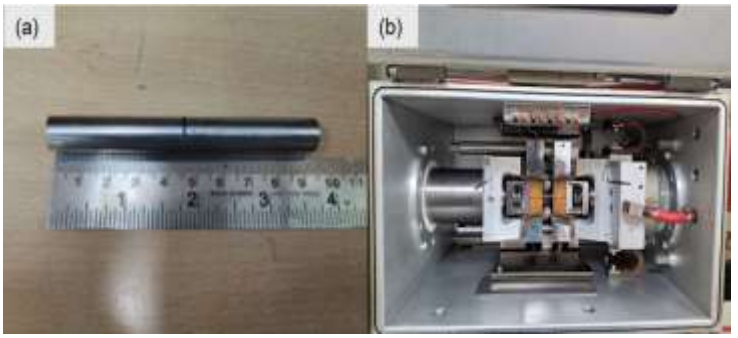


Figure 1: Photographs of (a) specimen deformed in compression test, and (b) chamber containing the specimen fixed between the copper grips in the Gleeble 3500 simulator. The photograph in (b) was taken after deformation.

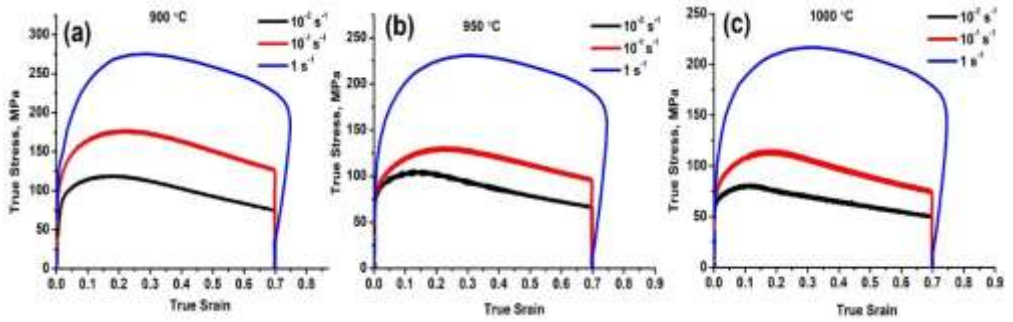


Figure 2: Stress-strain behaviour of AISI 4340 steel, captured during uniaxial compression.

strain rate) on the deformation stress are investigated with the aid of Zener-Hollomon parameter (Z) [15–18].

$$Z = \dot{\varepsilon}\exp\left(\frac{Q}{RT}\right) = A\sigma^{n} \quad (1)$$

$$= \dot{\varepsilon}\exp\left(\frac{Q}{RT}\right) = A'\exp(\beta.\sigma) \quad (2)$$

$$= \dot{\varepsilon}\exp\left(\frac{Q}{RT}\right) = A''[\sinh(\alpha.\sigma)]^{n'} \quad (3)$$

where Q is the activation energy (J/mol) of the deformation, and σ is the stress attained from the deformation flow curves. T denotes the temperature at which processing is carried out. The material constants and the activation energy are determined from the following equations derived from the aforementioned three equations.

$$\ln\sigma = \left(\frac{1}{n}\right)(\ln\dot{\varepsilon}) + \left(\frac{1}{n}\right)\left(\frac{Q}{RT} - \ln A\right) \quad (4)$$

$$\sigma = \left(\frac{1}{\beta}\right)(\ln\dot{\varepsilon}) + \left(\frac{1}{\beta}\right)\left(\frac{Q}{RT} - \ln A'\right) \quad (5)$$

$$\ln(\sinh(\alpha.\sigma p)) = \left(\frac{1}{n'}\right)(\ln\dot{\varepsilon}) + \left(\frac{1}{n'}\right)\left(\frac{Q}{RT} - \ln A''\right) \quad (6)$$

The material constants, namely, n, β, and n′, and Q are estimated from slopes of the curves in Fig. 3. The estimated average magnitudes of the material constants n, β, n′ are determined to be be 5.281, 0.033 $MPa^{-1}$, and 3.957 respectively. α (= β/n) was determined to be 0.0063 $MPa^{-}$

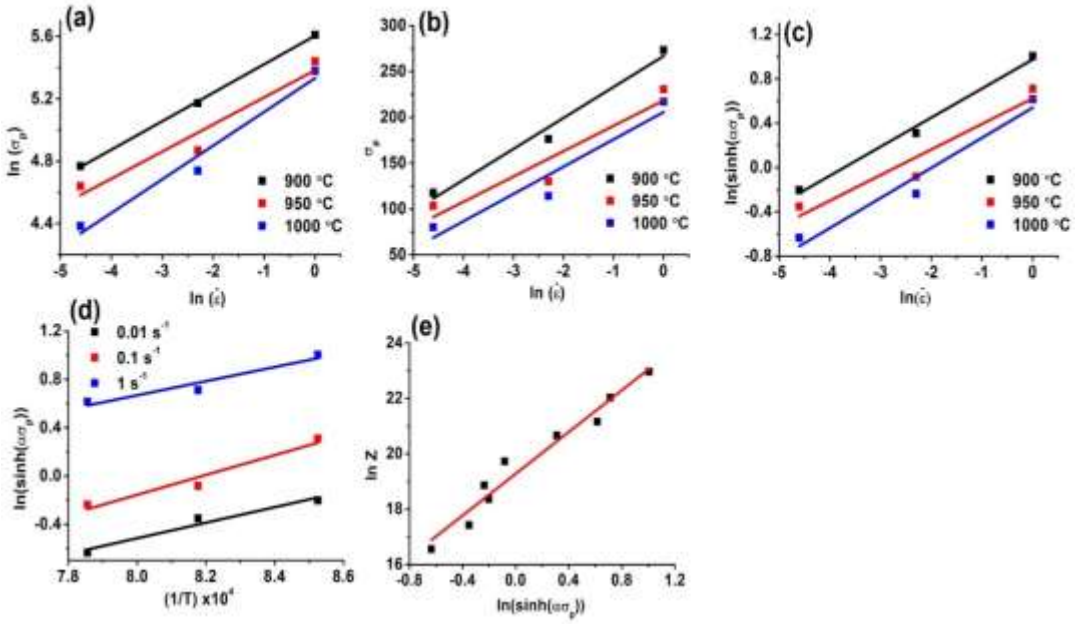


Figure 3: Variation of peak stress with deformation rate at different processing temperatures in (a), (b), and (c). Relationship between (d) peak stress and temperature, and (e) Zener-Hollomon parameter and peak stress.

[1]. The activation energy calculated using the slope of the curve (Fig. 3d) is estimated as 224 KJ/mol. The intercept of the curve (Fig. 3e) gives A″ as 2.36 x$10^8$. The constitutive equation is therefore determined to be $Z = 2.36 \times 10^8[\sinh(0.0063\sigma_p)]^{3.957} = \dot{\varepsilon} \exp(\frac{224000}{RT})$. The activation energy determined in the current study is 224 kJmol$^{-1}$ .

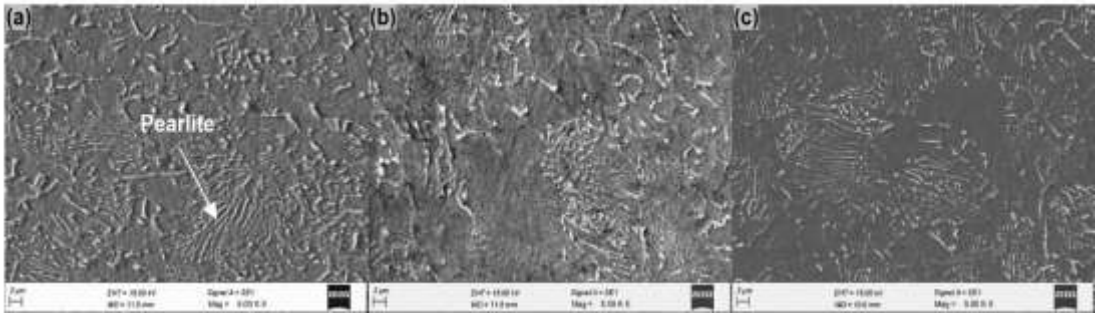


Figure 4: The microstructures of the 4340 alloy strained at (a) 900 °C, 0.1 s$^{-1}$, (b) 950 °C, 0.01 s$^{-1}$, and (d) 1000 °C, 0.1 s$^{-1}$.

The activation energy reported for medium carbon steels by some of the researchers varies between 427 kJmol$^{-1}$ and 270 kJmol$^{-1}$ [19–21]. The activation energy refers to the atom's ability to surmount various obstacles during processing [22]. Q is influenced by various processes like climb, cross-slip, chemical composition, nature of interfaces etc. [23].The lamellar structure in the attained structures ( Fig. 4) indicates the presence of pearlite in microstructure.

The flow stress-true plastic strain ($\varepsilon_P$) curves were fitted to Holloman (equation 7) and Ludwigson (equation 8) [12,24] models which describe the flow behaviour.

$$\sigma = K_H \varepsilon_P^{n_H} \quad (7)$$

$$\boldsymbol{\sigma = K_l \varepsilon_P^{n_l} + \exp(K_2 + n_2 \varepsilon_P)} \quad (8)$$

where $K_H$ and $K_l$ represent the strength coefficients, $n_H$ and $n_l$ represent the strain hardening exponents, and $K_2$ and $n_2$ are the coefficients that have been incorporated to take into account the deviation of experimental stress values from those predicted by Holloman model. The Ludwigson model fits the experimentally acquired flow stress-strain curves slightly better when compared to the Holloman model (Fig. 5), as evidenced by the attainment of lower chi-square ($\chi^2$) values when the experimental data is fitted to the former model (Table 1).

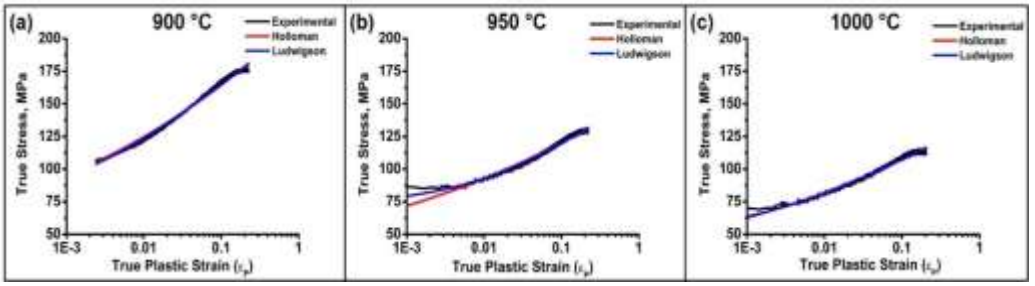


Figure 5: Ludwigson model fit to the flow curves of 4340 steel. All the curves depict the flow behaviour at 0.1 $s^{-1}$ (strain rate).

The strength coefficient ($K_1$) increased with elevation in strain rate at each of the deformation temperatures (Table 1). Thus, increasing the strain rate has contributed to a rise in the extent of strain hardening [12]. The hardness (Fig. 6) decreased with increase in temperature for each of the strain rates. The hardness was found to be lowest when the steel was strained at 1000 °C, 0.01 $s^{-1}$. The decrease in hardness can be ascribed to the occurrence of DRX [4]. The nucleation of recrystallization in the austenite phase begins when dislocation density value reaches the critical value, which is influenced by the temperature, strain rate, and strain [15]. Since austenite phase has low SFE, DRX is favoured as the cross-slip of dislocations is hindered. It is observed that at each of the deformation temperatures, the hardness increases when the strain rate associated with the deformation is varied from 0.01 to 0.1 $s^{-1}$. Such an increase in hardness can occur due to rise in dislocation density, and subsequent increased interaction between dislocations, with increase in strain rate [25].

Table 1. Holloman and Ludwigson parameters determined for hot deformed AISI 4340 steel

| Temperature (°C) and Strain rate ($s^{-1}$) | | Holloman | | | Ludwigson | | | | |
|---|---|---|---|---|---|---|---|---|---|
| | | n | K (MPa) | $\chi^2$ | $K_1$ (MPa) | $n_1$ | $K_2$ | $n_2$ | $\chi^2$ |
| 900 | 1 | 0.16 | 358 | 35.12 | 365 | 0.31 | 4.40 | -2.12 | 26.60 |
| | 0.1 | 0.12 | 217 | 4.87 | 217 | 0.23 | 3.94 | -2.84 | 2.73 |

| | | | | | | | | | |
|---|---|---|---|---|---|---|---|---|---|
| | 0.01 | 0.08 | 139 | 0.98 | 133 | 0.37 | 4.30 | -2.12 | 0.45 |
| 950 | 1 | 0.16 | 288 | 19.85 | 287 | 0.23 | 3.65 | -2.38 | 16.89 |
| | 0.1 | 0.11 | 155 | 3.54 | 151 | 0.40 | 4.24 | -1.61 | 1.49 |
| | 0.01 | 0.06 | 118 | 1.41 | 115 | 0.43 | 4.30 | -2.05 | 0.78 |
| 1000 | 1 | 0.15 | 271 | 16.92 | 273 | 0.25 | 3.88 | -2.37 | 12.41 |
| | 0.1 | 0.12 | 140 | 2.22 | 137 | 0.26 | 3.73 | -2.42 | 1.58 |
| | 0.01 | 0.05 | 91 | 1.04 | 97 | 0.51 | 4.13 | -2.06 | 1.23 |

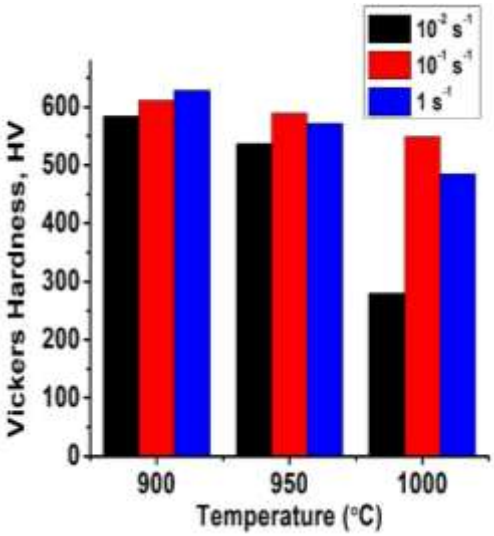


Figure 6: Vickers Hardness of AISI 4340 steel deformed at different deformation rates

**Conclusions**

The AISI 4340 steel was subjected to elevated temperature uniaxial compression at various deformation velocities. The constitutive equation, which relates the flow stress with processing parameters was determined. Additionally, the microstructural characterization of the deformed steel and hardness tests on the deformed structures were carried out. The rise in peak stress and peak strain resulted from an increase in strain rate from the lowest ($10^{-2}$ $s^{-1}$) to the highest (1 $s^{-1}$) at each of the deformation temperatures. The constitutive equation was found to be $2.36 \times 10^{8}[\sinh(0.0063\sigma_p)]^{3.957} = \dot{\varepsilon} \exp(\frac{224000}{RT})$. The Ludwigson model offered better fit to the

experimental stress-strain curves compared to the Holloman model. Hardness was found to be lower for the steel deformed at higher temperatures.

**Acknowledgment**
The authors would like to acknowledge the support provided by the Management of PSG College of Technology, Coimbatore, and Dr. R. Sivasankari, Assistant Professor (Sl. Gr.), Metallurgical Engineering, PSG College of Technology for conducting the experiments in Gleeble® 3500.

## Reference

[1] W.B. Rashid, S. Goel, X. Luo, J.M. Ritchie, An experimental investigation for the improvement of attainable surface roughness during hard turning process, Proceedings of the Institution of Mechanical Engineers, Part B: Journal of Engineering Manufacture 227 (2013) 338–342. https://doi.org/10.1177/0954405412464217.

[2] A.-S.G. Abdel-Salam, A. Sohail, L. Sherin, Q.U.A. Azim, A. Faisal, M.A. Fahmy, Z. Li, Optimization of tank engine crank shaft material properties, Mechanics Based Design of Structures and Machines 51 (2023) 3066–3082. https://doi.org/10.1080/15397734.2021.1916754.

[3] V. Singh, G.G. Roy, P. Srirangam, D. Chakrabarti, A.K. Agarwal, Study of Hot Deformation Behavior of EN25 Steel in the Presence of Non-metallic Inclusions, J. of Materi Eng and Perform 33 (2024) 3320–3337. https://doi.org/10.1007/s11665-024-09247-3.

[4] S. Kingklang, V. Uthaisangsuk, Investigation of Hot Deformation Behavior of Duplex Stainless Steel Grade 2507, Metall Mater Trans A 48 (2017) 95–108. https://doi.org/10.1007/s11661-016-3829-4.

[5] M. Khan, D. Shahriari, M. Jahazi, J.-B. Morin, Interactions Between Dynamic Softening and Strengthening Mechanisms During Hot Forging of a High-Strength Steel, Front. Mech. Eng. 7 (2021) 697116. https://doi.org/10.3389/fmech.2021.697116.

[6] V. Singh, P. Srirangam, D. Chakrabarti, G.G. Roy, Hot Deformation Behavior of EN30B Forged Steels in the Presence of Non-metallic Inclusions, J. of Materi Eng and Perform 32 (2023) 10885–10897. https://doi.org/10.1007/s11665-023-07800-0.

[7] J. Park, Y. Kim, S. Shin, N. Kim, Characterization of Hot Workability in AISI 4340 Based on a 3D Processing Map, Metals 12 (2022) 1946. https://doi.org/10.3390/met12111946.

[8] H.Y. Jeong, J. Park, Y. Kim, S.Y. Shin, N. Kim, Processing parameters optimization in hot forging of AISI 4340 steel using instability map and reinforcement learning, Journal of Materials Research and Technology 23 (2023) 1995–2009. https://doi.org/10.1016/j.jmrt.2023.01.106.

[9] A. Łukaszek-Sołek, J. Krawczyk, T. Śleboda, J. Grelowski, Optimization of the hot forging parameters for 4340 steel by processing maps, Journal of Materials Research and Technology 8 (2019) 3281–3290. https://doi.org/10.1016/j.jmrt.2019.05.018.

[10] E. Alibeiki, J. Rajabi, Investigation of Flow Stress Behavior of AISI 4340 Steel in Thermomechanical Process, Jurnal Kejuruteraan 32 (2020) 25–30. https://doi.org/10.17576/jkukm-2020-32(1)-04.

[11] A. Sanrutsadakorn, V. Uthaisangsuk, S. Suranuntchai, Determination of Initiation of Dynamic Recrystallization in AISI 4340 Steel, AMR 893 (2014) 381–386. https://doi.org/10.4028/www.scientific.net/AMR.893.381.

[12] A. Lavakumar, S.S. Sarangi, V. Chilla, D. Narsimhachary, R.K. Ray, A "new" empirical equation to describe the strain hardening behavior of steels and other metallic materials, Materials Science and Engineering: A 802 (2021) 140641. https://doi.org/10.1016/j.msea.2020.140641.

[13] X.-M. Chen, Y.C. Lin, D.-X. Wen, J.-L. Zhang, M. He, Dynamic recrystallization behavior of a typical nickel-based superalloy during hot deformation, Materials & Design 57 (2014) 568–577. https://doi.org/10.1016/j.matdes.2013.12.072.

[14] D.-X. Wen, Y.C. Lin, Y. Zhou, A new dynamic recrystallization kinetics model for a Nb containing Ni-Fe-Cr-base superalloy considering influences of initial δ phase, Vacuum 141 (2017) 316–327. https://doi.org/10.1016/j.vacuum.2017.04.030.

[15] T.R. Dandekar, R.K. Khatirkar, A. Gupta, N. Bibhanshu, A. Bhadauria, S. Suwas, Strain rate sensitivity behaviour of Fe–21Cr-1.5Ni–5Mn alloy and its constitutive modelling, Materials Chemistry and Physics 271 (2021) 124948. https://doi.org/10.1016/j.matchemphys.2021.124948.

[16] B. Guo, H. Ji, X. Liu, L. Gao, R. Dong, M. Jin, Q. Zhang, Research on Flow Stress During Hot Deformation Process and Processing Map for 316LN Austenitic Stainless Steel, J. of Materi Eng and Perform 21 (2012) 1455–1461. https://doi.org/10.1007/s11665-011-0031-0.

[17] S. Zangeneh Najafi, A. Momeni, H.R. Jafarian, S. Ghadar, Recrystallization, precipitation and flow behavior of D3 tool steel under hot working condition, Materials Characterization 132 (2017) 437–447. https://doi.org/10.1016/j.matchar.2017.09.009.

[18] Y. Zhou, Y. Liu, X. Zhou, C. Liu, L. Yu, C. Li, B. Ning, Processing maps and microstructural evolution of the type 347H austenitic heat-resistant stainless steel, J. Mater. Res. 30 (2015) 2090–2100. https://doi.org/10.1557/jmr.2015.168.

[19] S.V. Sajadifar, G.G. Yapici, M. Ketabchi, B. Bemanizadeh, High Temperature Deformation Behavior of 4340 Steel: Activation Energy Calculation and Modeling of Flow Response, J. Iron Steel Res. Int. 20 (2013) 133–139. https://doi.org/10.1016/S1006-706X(13)60226-5.

[20] M. Eckert, M. Krbata, I. Barenyi, J. Majerik, A. Dubec, M. Bokes, Effect of Selected Cooling and Deformation Parameters on the Structure and Properties of AISI 4340 Steel, Materials 13 (2020) 5585. https://doi.org/10.3390/ma13235585.

[21] J.M. Cabrera, A. Al Omar, J.M. Prado, J.J. Jonas, Modeling the flow behavior of a medium carbon microalloyed steel under hot working conditions, Metall Mater Trans A 28 (1997) 2233–2244. https://doi.org/10.1007/s11661-997-0181-8.

[22] P. Zhou, L. Deng, M. Zhang, P. Gong, X. Wang, Characterization of Hot Workability of 5052 Aluminum Alloy Based on Activation Energy-Processing Map, J. of Materi Eng and Perform 28 (2019) 6209–6218. https://doi.org/10.1007/s11665-019-04367-7.

[23] T.R. Dandekar, R.K. Khatirkar, A. Gupta, N. Bibhanshu, A. Bhadauria, S. Suwas, Strain rate sensitivity behaviour of Fe–21Cr-1.5Ni–5Mn alloy and its constitutive modelling, Materials Chemistry and Physics 271 (2021) 124948. https://doi.org/10.1016/j.matchemphys.2021.124948.

[24] V.D. Vijayanand, K. Laha, P. Parameswaran, M. Nandagopal, S. Panneer Selvi, M.D. Mathew, Influence of thermo-mechanical treatment on the tensile properties of a modified 14Cr–15Ni stainless steel, Journal of Nuclear Materials 453 (2014) 188–195. https://doi.org/10.1016/j.jnucmat.2014.06.067.

[25] B. Gu, P. Chekhonin, S.W. Xin, G.Q. Liu, C.L. Ma, L. Zhou, W. Skrotzki, Effect of temperature and strain rate on the deformation behavior of Ti5321 during hot-compression, Journal of Alloys and Compounds 876 (2021) 159938. https://doi.org/10.1016/j.jallcom.2021.159938.